On the maneuvering control of networks of moving vehicles

Jae Park

Faculty of Systems Engineering, Jungwon University, Goesan, Korea
Email: japark82@jwu.ac.kr

Evgeniy Grechnikov

Department of Mathematics, Bauman Moscow State Technical University, Moscow, Russia
Email: grechnikov@gmail.com

Fang Chen

Department of Mathematics and Computer Sciences, Xinjiang Normal University, Urumchi 830054, China
Email: chenfang@stu.xjnu.edu.cn

Abstract: This paper discusses the maneuvering control algorithm based on all-wheel independent driving and steering control techniques for special purpose 6WD/WS vehicles. The maneuvering control algorithms considering superior dynamic characteristics of high power in-wheel motors and independent steering system are designed to perform driving and steering control, vehicle stability control, and fault tolerant control. The maneuvering controller applies sliding and optimal control theories considering optimal torque distribution and friction circle related to the vertical tire force. The fault tolerant control algorithm is applied to obtain the similar maneuverability to that of the non-faulty vehicle. The simulations using the Matlab/Simulink model and experiments using HIL simulator with the designed control algorithms prove the remarkably improved performances in terms of vehicle stability and maneuverability under the double lane change, slalom, and fish-hook test conditions.

Key-Words: All-wheel independent control, Fault tolerant control, Friction circle, Maneuvering controller, Vehicle stability control

1 Introduction

The multi-axis electric propulsion system with high power in-wheel motors and independent steering motors is a new advanced concept to perform military missions successfully as well as to enhance maneuverability and survivability. Wheeled vehicles based on independent wheel driving and steering control has been developed to perform special purpose missions on off-road and extreme terrains.

A great deal of studies have been undertaken extensively to find a proper control method which can give good maneuverability and stability for four-wheeled vehicles [1][2]. However, there has not been considerable research effort to develop maneuvering control algorithm related to vehicle stability and fault tolerant control for six-wheeled vehicles. Jackson proposed the yaw rate control method using direct yaw moment control to improve the stability of their six-wheeled vehicle when turning a corner [3]. And, Kim proposed the drive control system design methods to improve the stability and maneuverability of a 6WD/6WS vehicle [4]. Han researched control methods improving the vehicle behavior by using optimization methods of longitudinal and lateral tire forces for six-wheeled vehicles [5]. Also, Lee developed the maneuvering control system based on all-wheel independent driving and steering control for special purpose vehicles and proved the performances with simulations [6].

In order to research the maneuvering control algorithms of 6WD/6WD vehicle, the test platform equipped with in-wheel driving system, dual braking system, hybrid steering system and a maneuvering controller is developed to test and evaluate the maneuvering control algorithm. In this paper, the control algorithm to accomplish effective maneuvering control, high speed stability control, and fault tolerant control are developed based on high dynamic characteristics of in-wheel motor module and advantages of independent steering and driving. A maneuvering controller with control algorithms consists of driving controller (upper and lower level controllers) and fault tolerant controller.

2 Vehicle Dynamics Model

The 6WD/6WS vehicle dynamics model which is consisted of body dynamics, driving system,

suspension and vertical tire forces models is developed using Matlab/Simulink. The six-wheeled vehicle with individual driving and steering control is modeled as an object with 18 degree-of-freedom as shown in Fig.1. The full vehicle model consists of six DOF (translational and rotational) dynamic models of the sprung mass, six suspension models and six wheel dynamics.
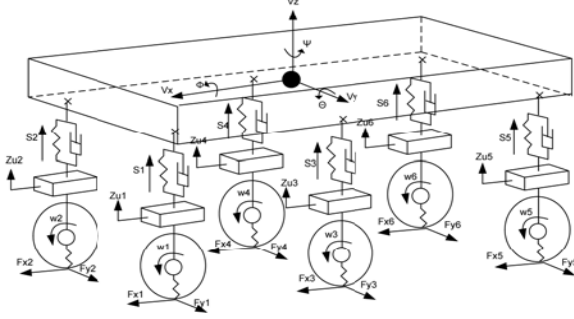

Fig.1 Dynamics model of 6WD/6WS vehicle

Table 1. Parameter values of 6WD/WS Vehicle

Parameter	Value
Sprung mass (m_s)	7200 [kg]
Unsprung mass (m_u)	262 [kg]
Wheel base(L)	3.180[m]
Length from C.G to i-th wheel axis($l_{\#i}$)	1.382 [m]
	0.268 [m]
	1.798 [m]
Moment of inertia (I_z)	37,303 [kg-m^2]
Wheel moment of inertia (J_w)	51 [kg-m^2]
Suspension spring stiffness (K_t)	80,000 [N/m]
Tire stiffness (K_r)	560,000 [N/m]
Steering column inertia (I_h)	0.035 [kg-m^2]
Steering column stiffness (K_i)	50,000 [Nm/rad]
Wheel tread of i-th wheel axis ($t_{\#i}$)	2.296 [m]
Height from tire contact point to C.G($h_{\#i}$)	1.107 [m]
Tire radius(r_i)	0.560 [m]

The behavior of sprung mass are determined by steering input, and tire and suspension forces of longitudinal and lateral directions. Force and moment equations of sprung mass illustrated in Fig.1 are derived as Eq.(1) and (2) by applying Newton and Euler equations. Where, M_s is the vehicle total mass, which is sprung mass(m_s) plus unsprung mass(m_u).

$$\sum F = Ma_G$$

$$\sum F_x = M_s(a_x + v_z w_y - v_y w_z)$$
$$\sum F_y = M_s(a_y + v_x w_z - v_z w_x)$$
$$\sum F_z = M_s(a_z + v_y w_x - v_x w_y)$$

(1)

$$\sum M = \dot{H}_g$$

$$\sum M_x = I_x a_x + (I_z - I_y)w_y w_z$$
$$\sum M_y = I_y a_y + (I_x - I_y)w_z w_x$$
$$\sum M_z = I_z a_z + (I_y - I_x)w_x w_y$$

(2)

The total net tire forces of longitudinal and lateral directions are calculated as Eq.(3) and (4).

$$\sum F_x = \sum_{i=1}^{6} F_{i\_tirex} \cos(\gamma_i) - \sum_{i=1}^{6} F_{i\_tirey} \sin(\gamma_i)$$

(3)
$$\sum F_y = \sum_{i=1}^{6} F_{i\_tirey} \cos(\gamma_i) + \sum_{i=1}^{6} F_{i\_tirex} \sin(\gamma_i)$$

(4)

On the other hands, the total net moment of x, y, z directions, that is generated by tire forces of *x* and *y* directions and loads applied to individual tires, are represented as Eq.(5), (6), and (7), respectively.

$$\sum M_x = h_{\#1}\left[\sum_{i=1}^{2} F_{i\_tirex} \sin(\gamma_i) + \sum_{i=1}^{2} F_{i\_tirey} \cos(\gamma_i)\right]$$
$$+ h_{\#2}\left[\sum_{i=3}^{4} F_{i\_tirex} \sin(\gamma_i) + \sum_{i=3}^{4} F_{i\_tirey} \cos(\gamma_i)\right]$$
$$+ h_{\#3}\left[\sum_{i=5}^{6} F_{i\_tirey}\right]$$
$$+ \frac{t_{\#1}}{2}(F_{s1} - F_{s2}) + \frac{t_{\#2}}{2}(F_{s3} - F_{s4}) + \frac{t_{\#3}}{2}(F_{s5} - F_{s6})$$

(5)

$$\sum M_y = h_{\#1}\left[\begin{array}{l} F_{1\_tirey} \sin(\gamma_1) - F_{1\_tirex} \cos(\gamma_1) + F_{3\_tirey} \sin(\gamma_3) \\ -F_{3\_tirex} \cos(\gamma_3) - F_{5\_tirex} \end{array}\right]$$
$$+ h_{\#2}\left[\begin{array}{l} F_{2\_tirey} \sin(\gamma_2) - F_{2\_tirex} \cos(\gamma_2) + F_{4\_tirey} \sin(\gamma_4) \\ -F_{4\_tirex} \cos(\gamma_4) - F_{6\_tirex} \end{array}\right]$$
$$- l_{\#1}\sum_{i=1}^{2} F_{si} - l_{\#2}\sum_{i=3}^{4} F_{si} + l_{\#3}\sum_{i=5}^{6} F_{si}$$

(6)

$$\sum M_z = l_{\#1}\sum_{i=1}^{2}[F_{itirey} \cdot \cos(\gamma_i) + F_{itirex} \cdot \sin(\gamma_i)]$$
$$+ l_{\#2}\sum_{i=3}^{4}[F_{itirey} \cdot \cos(\gamma_i) + F_{itirex} \cdot \sin(\gamma_i)] - l_{\#3}\sum_{i=5}^{6} F_{itirey}$$
$$+ \frac{t_{\#1}}{2}[-F_{1tirex} \cdot \cos(\gamma_1) + F_{1tirey} \cdot \sin(\gamma_2) + F_{2tirex} \cdot \cos(\gamma_3)]$$
$$+ \frac{t_{\#2}}{2}[-F_{3tirex} \cdot \cos(\gamma_3) + F_{3tirey} \cdot \sin(\gamma_3) + F_{4tirex} \cdot \cos(\gamma_4)]$$
$$+ \frac{t_{\#3}}{2}[-F_{5tirex} + F_{6tirex}] - \sum_{i=1}^{6} M_{itirez}$$

(7)

The driving System model is consisted of wheel dynamics, longitudinal tire dynamics and lateral tire dynamics. In conventional propulsion systems, the drive force from the engine is transmitted to the wheels through the transmission. Whereas, in this electric propulsion system, the in-wheel motors generate the desired torques and supply drive powers to the wheels directly. Then, the applied power (torque) is transformed to angular acceleration to the wheels. Therefore, the wheel dynamic equation is derived as Eq.(8). J_w represents the wheel moment of inertia.

$$J_w \cdot \frac{d\omega_i}{dt} = T_i - r_i \cdot F_{i\_tirex} \qquad (8)$$

The angular acceleration of the wheel is determined in accordance with applied power and

slip condition of the ground. The relationship of the input to output torques of motors are represented by the first order time delay response with time constant(τ_m) as Eq.(9).

$$\frac{T_{out}}{T_{com}} = \frac{1}{1 + \tau_m \cdot s} \tag{9}$$

In the real system, the longitudinal tire forces are determined by friction between the ground and the tire. The slip ratio can be obtained from the vehicle velocity determined in body dynamics and the wheel velocity determined in wheel dynamics. The wheel slip ratio (λ_i) of each wheel is calculated as Eq.(10). And the slip angle (α_i) of the tire is defined as Eq.(11). Where, v_i and ξ_i represent wheel velocity and included angle, respectively.

$$\lambda_i = \begin{cases} \dfrac{r_i \cdot \omega_i - v_i \cos \alpha_i}{r_i \cdot \omega_i} & if \left(\lambda_i > 0 \right) \\ \dfrac{r_i \cdot \omega_i - v_i \cos \alpha_i}{v_i \cos \alpha_i} & if \left(\lambda_i \le 0 \right) \end{cases}$$

$$(10)$$

$$\alpha_i = \delta_i - \xi_i$$

$$(11)$$

3 Maneuvering Control Algorithm

Maneuvering control systems perform driving control(drive, steer, and brake), high speed stability control(lateral, rollover, attitude), and fault tolerant control(controller, senor, and actuator faulted) based on high dynamic response of in-wheel motors, independent wheel drive, and steer control. The integrated maneuvering control algorithm shown in Fig.2 is consisted of driving control, high speed stability control, and fault tolerant control algorithms.
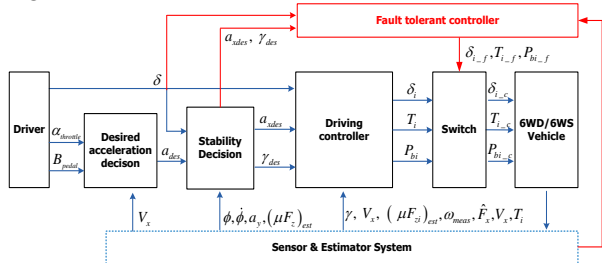

Fig. 2 Block diagram of integrated maneuvering control algorithm

Fig.3 shows the driving controller block diagram consists of upper and lower level controllers. Based on yaw rate control of vehicle z axis rotation, the vehicle velocity control, high speed stability control, rollover prevention control, and slip rate control algorithms are implemented to enhance the maneuvering performance and ensure the stability.
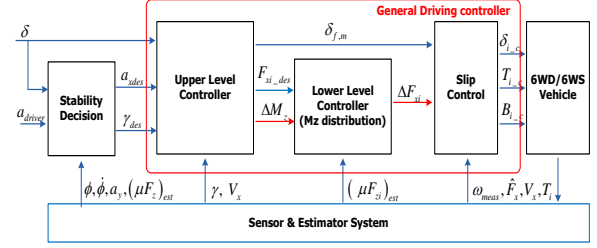

Fig. 3. Block diagram of driving controller

The upper level controller based on sliding control theory determines front, middle, and rear steering angles, additional net yaw moment, and longitudinal net force depending on the reference velocity and steering angle. According to the driver's steering angle the desired yaw rate and yaw moment are determined by measuring yaw rate based on sliding mode control as shown in Fig.4. And the desired longitudinal force can be obtained with the difference between desired and real acceleration is determined.
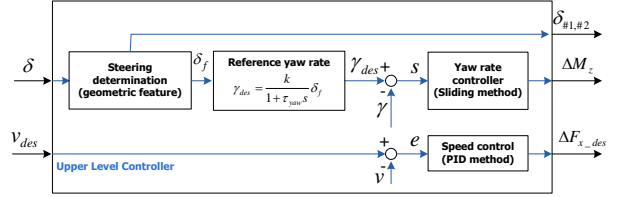

Fig. 4. Block diagram of upper level controller

The desired longitudinal net force based on PID control to satisfy desired vehicle velocity can be calculated by Eq.(12).

$$F_{x\_des} = m \cdot a_{des} = m \cdot \begin{bmatrix} K_p (v_{des} - v_x) \\ + K_I \int (v_{des} - v_x) dt + K_d \dfrac{d(v_{des} - v_x)}{dt} \end{bmatrix} \tag{12}$$

The desired yaw moment to satisfy desired vehicle yaw rate determined by stability controller based on sliding mode control theory suitable for fast responses and nonlinear dynamic behaviors of the vehicle is calculated by Eq.(13).

$$\Delta M_z = -2l_f F_{yf} \cos \delta_f - 2l_m F_{ym} \cos \delta_m$$

$$+ 2l_r F_{yr} + \hat{I}_z \cdot \dot{\gamma}_d + \hat{I}_z k sat \left(\frac{s}{\Phi} \right) \tag{13}$$

The lower level controller is designed to distribute the additional front lateral tire force and longitudinal tire forces at each wheel in order to satisfy the desired longitudinal net force and yaw moment calculated by the upper level controller. The distributed longitudinal and lateral tire forces are determined as proportion to the size of the friction circle according to the change in driving conditions. The slip controller determines the input torque so that slippage does not occur by monitoring the state of each wheel.
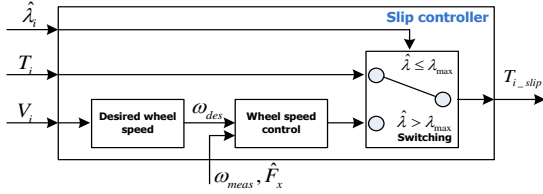
Fig. 5. Block diagram of wheel slip control algorithm

The friction circle is defined as the maximum tire force that can be generated on each wheel. The control strategy determines the additional front lateral tire forces, and differential traction and braking forces of all six wheels according to the friction circle as shown in Fig.6.
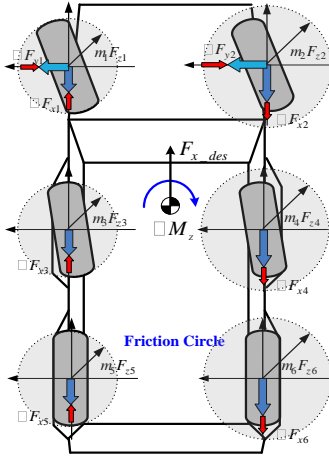

Fig. 6. Optimal torque distribution strategy of lower level controller

The performance index is composed of numerous combinations of control inputs. The control inputs are selected to minimize the value of the proposed performance index shown in Eq.(14). The minimum additional inputs are determined by the tire force that is currently applied, and the minimum additional inputs are proportional to the size of friction circles.

$$J = \frac{c_{x1}\Delta F_{x1}^{\ 2}}{(\mu_1 F_{z1})^2} + \frac{c_{x2}\Delta F_{x2}^{\ 2}}{(\mu_2 F_{z2})^2} + \frac{c_{x3}\Delta F_{x3}^{\ 2}}{(\mu_3 F_{z3})^2}$$
$$+ \frac{c_{x4}\Delta F_{x4}^{\ 2}}{(\mu_4 F_{z4})^2} + \frac{c_{x5}\Delta F_{x5}^{\ 2}}{(\mu_5 F_{z5})^2} + \frac{c_{x6}\Delta F_{x6}^{\ 2}}{(\mu_6 F_{z6})^2} \quad (14)$$

The longitudinal and additional lateral tire forces to be distributed should satisfy constraints shown in Eq.(15) and (16) related to the desired yaw moment and additional longitudinal tire net force.

$$F_{x\_des} = \Delta F_{x1} + \Delta F_{x2} + \Delta F_{x3} + \Delta F_{x4} + \Delta F_{x5} + \Delta F_{x6}$$
(15)

$$\Delta Mz = \frac{t}{2}\{-\Delta F_{x1} + \Delta F_{x2} - \Delta F_{x3} + \Delta F_{x4} - \Delta F_{x5} + \Delta F_{x6}\}$$
(16)

The high-speed stability control algorithm defines the desired lateral acceleration and yaw rate to secure the lateral stability and to prevent rollovers. The stability region is defined to ensure lateral stability and prevent rollovers. And lateral stability as well as rollover prevention is achieved by limiting the lateral acceleration.

The fault diagnosis and tolerant control functions are required in accordance with maneuvering control sensor and actuator failures. Furthermore, due to applying steer-by-wire system, the importance of system robustness is growing due to depending on sensor signals without mechanical connections between the driver's operating interfaces and actuators.

4 Simulations and Experiments

The performance characteristics of 6WD/6WS vehicle implemented with maneuvering controller are evaluated through simulations using Matlab/Simulink models and HIL simulators. HILS is composed of the same components and inner spaces as a real vehicle. The vehicle dynamics model and control algorithm are interconnected with real components as shown in Fig.7.

Fig. 7. Control algorithm test using HIL simulator

The double lane change simulation to evaluate the control performance of the maneuvering controller was performed with a high friction road condition (μ=0.85) at an initial vehicle speed of 60 km/h. Fig.8 shows simulation results with respect to stability control method such as no control(equal torque input), dual control(stability control through hybrid steering), and slip control(stability control through hybrid steering plus slip control). The dual and slip control algorithms enhance performance over that of the no control case with respect to the yaw rate error and lateral error as shown in Fig.8(a) and (b). The slip ratio with slip control is significantly smaller than that of the no control case and dual control case which is shown in Fig.8(c). As shown in Fig.8(d), the stability control performance can be verified with the vehicle trajectory trying to follow the desired trajectory compared to the no control case.

(a) Yaw rate error

(b) Lateral error
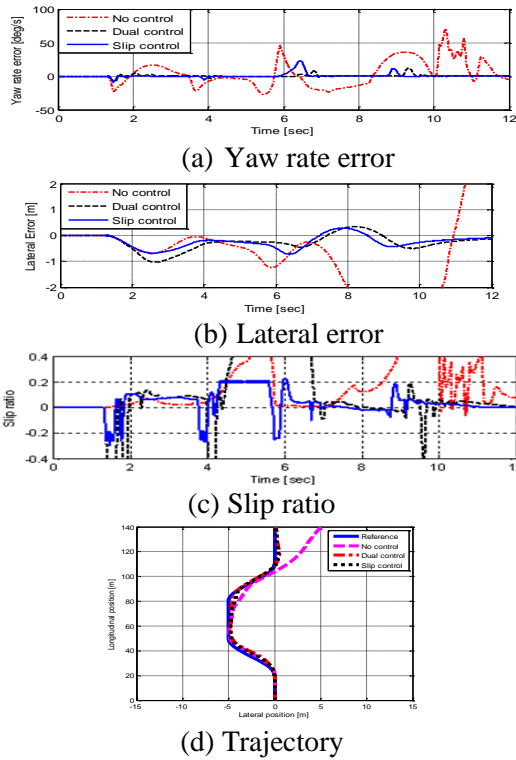

(c) Slip ratio

(d) Trajectory

Fig. 8. Simulation results of double lane change test depending on stability control method

The double lane change simulation to evaluate high-speed stability and rollover prevention performance was performed with the same conditions as Fig.8. Fig.9 shows simulation results with respect to vehicle stability control methods such as even distribution of drive torque(case I) and lateral stability control(case II). The driver model tracking the defined road determines steering inputs and the drive controller determines the required input torque of each wheel by calculating the desired force and moment values. In case of no stability control, the vehicle deviates from the defined path and fails to track the desired lane as shown in Fig.9(a). In this situation, the yaw rate error and lateral error increase significantly as shown in Fig.9(b) and (c).

(a) Trajectory

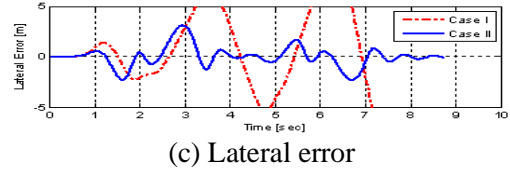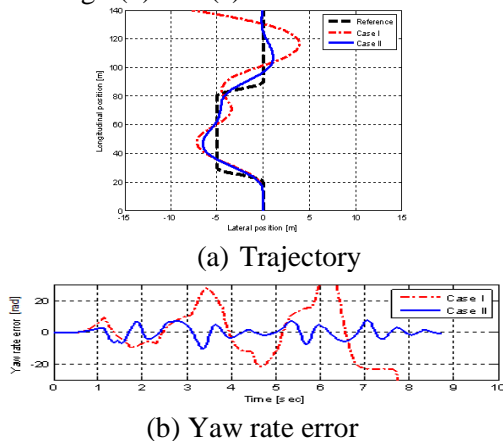(b) Yaw rate error

(c) Lateral error

Fig. 9. Simulation results of double lane change test depending on torque distribution method

The fish hook test simulation was performed with a high friction road condition(μ =0.85) at an initial vehicle speed of 80 km/h. And the driver's steering angle changes from 0° to 300° and then to -300° as shown in Fig.10(a). In case of no stability control(case I), the vehicle rolls over due to the excessive lateral acceleration and the red dotted line(longitudinal velocity) disappears as shown in Fig.10(b). The rollover index diverges as shown in Fig.10(c). But In case of the stability control(case II) the vehicle velocity decreases to lower stable level and the rollover do not occur because of rollover index maintaining constant value below 1 as shown in Fig.10(b) and (c).

(a) Steering angle
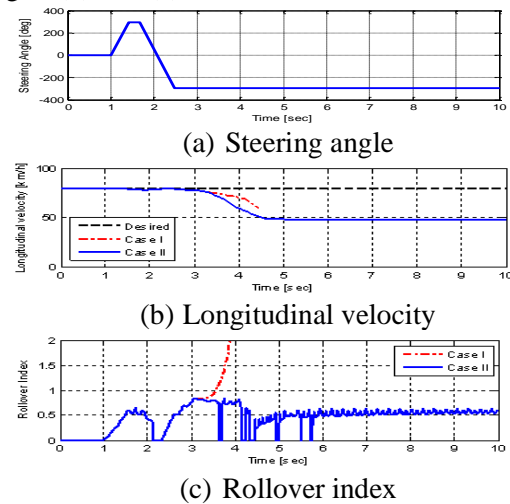

(b) Longitudinal velocity

(c) Rollover index

Fig. 10. Simulation results of fish-hook test depending on stability control algorithm

The double lane change simulation is performed with a failure condition of front wheel 1. The initial vehicle speed is 40 km/h and the steering angle of the front wheel is 10°. In the event of failure of one front wheel, the angle of steering mechanism acting on opposite direction is to be -10° while another front wheel maintains 10°. In this case, the vehicle velocity decreases remarkably, and the lateral error and yaw rate deviates unstably due to the increase of wheel slip by the driver's excessive input and more torque distribution than the torque limit of the lower level controller as shown in Fig.11(b), (c), and (d). But, as the desired yaw rate is restricted by applying the fault tolerant control method of the upper level

controller, the stable maneuver is mostly possible despite of rapid lane changes shown in Fig.11.

(a) Steering angle

(b) Vehicle longitudinal velocity
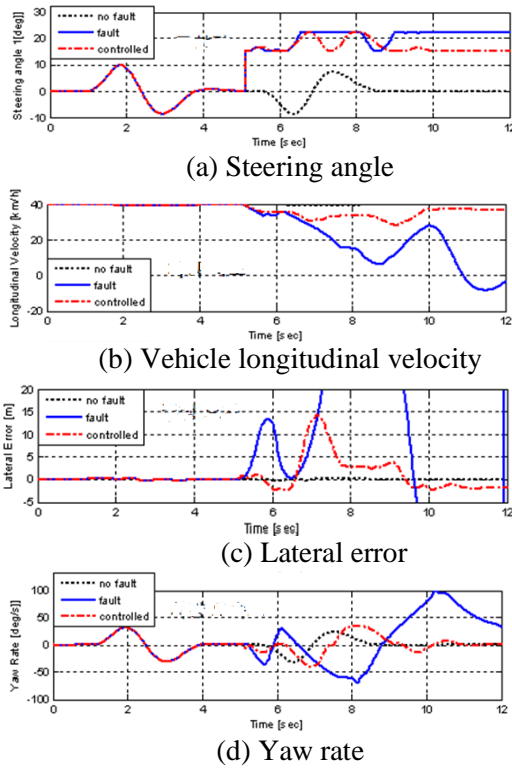

(c) Lateral error

(d) Yaw rate

Fig. 11. Simulation results depending on fault tolerant control algorithm

The performance tests of the control algorithm are performed using a HIL simulator as shown in Fig.7. In the case where vehicle velocity is 20km/h and 40km/h, double lane change and slalom tests are performed, respectively. The double lane change tests with the test course specified in ISO represent stable maneuvering over 40km/h as shown in Fig.12. The test vehicle follows the given test course without excessive yaw rate and lateral acceleration by applying vehicle stability control algorithm.

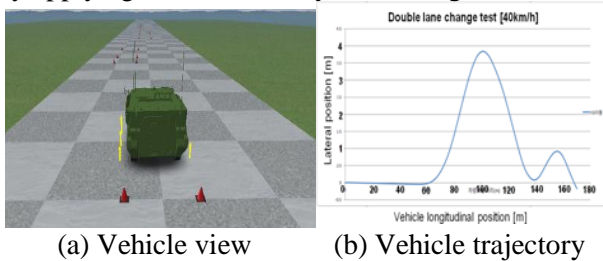(a) Vehicle view   (b) Vehicle trajectory
Fig. 12. Double lane change test results using HILS

The slalom tests with the test course specified in JASO represent stable maneuvering over 40km/h as shown in Fig.13. Also, the test vehicle follows the given test course without excessive yaw rate, lateral velocity, and lateral acceleration by applying vehicle stability control algorithm. However, the magnitude of vehicle maneuvering stability elements such as yaw rate, roll angle, roll rate, lateral velocity, and lateral acceleration increase rapidly compared to that of the double lane change test results.
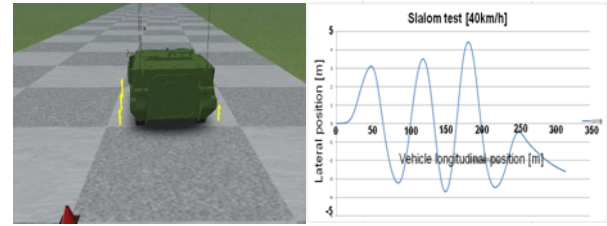

(a) Vehicle view   (b) Vehicle trajectory
Fig. 13. Slalom test results using HILS

5 Conclusion

A maneuvering control algorithm based on the independent all-wheel driving and steering control has been proposed to improve the maneuverability and survivability for special purpose 6WD/6WS vehicles. The control algorithm to perform maneuvering, high speed stability, and fault tolerant controls effectively are derived based on high dynamic characteristics of in-wheel motor and advantages of independent steer and drive. The maneuvering controller applies sliding and optimal control theories considering optimal torque distribution and friction circle related to the vertical tire force. The maneuvering performance of the 6WD/6WS vehicle with these maneuvering control algorithms have been evaluated by simulations using Matlab/Simulink and experiments using a HIL simulator subjected to double lane change, fish-hook, and slalom tests. The simulation and experiment results of these designed control algorithms prove the improved performances compared to conventional controller in terms of vehicle stability and maneuverability.

References:
[1] M. Nagai, Y. Hirano, and S. Yamanaka, Integrated Control of Active Rear Wheel Steering and Direct Yaw Moment Control, *J. of Vehicle System Dynamics*, vol.27, 1997, pp.357-370.
[2] O. Mokhiamar and M. Abe, Simultaneous Optimal Distribution of Lateral and Longitudinal Tire Forces for the Model Following Control, *J. of Dynamic Systems, Measurement, and Control*, vol.126, 2004, pp.753-763.
[3] A. Jackson, and D. Crolla, Improving Performance of a 6x6 Off-road Vehicle Through Individual Wheel Control, *SAE Paper No. 2002-01-0968*, 2002.
[4] W.G. Kim, J.Y. Kang, and K. Yi, Drive Control System Design for Stability and Maneuverability of a 6WD/6WS Vehicle, *Int. J.*

of Automotive Technology, Vol.12, No.1, 2011, pp.67-74.

[5] C.J. Kim and C.S. Han, A Study on Independent Steering & Driving Control Algorithm for 6WS/6WD Vehicle, *Journal of Institute of Control, Robotics and Systems*, Vol.17, No.4, 2011, pp.313-320.

[6] D.O. Lee, S.T. Yeo, J.S. Lee, W.G. Kim, and J.W. Na, A Study on Maneuvering Control System Design Based on All-wheel Independent Driving and Steering Control Approach for Special Purpose Vehicles, *Proceedings of KIMST conference*, 2012, pp.1931-1934.